ACS Photonics

pubs.acs.org/journal/apchd5

Letter

Enhanced Plasmonic Photocatalysis through Synergistic Plasmonic–Photonic Hybridization

Qinglan Huang, Taylor D. Canady, Rohit Gupta, Nantao Li, Srikanth Singamaneni, and Brian T. Cunningham*

Cite This: https://dx.doi.org/10.1021/acsphotonics.0c00945

Read Online

ACCESS | Metrics & More | Article Recommendations | Supporting Information

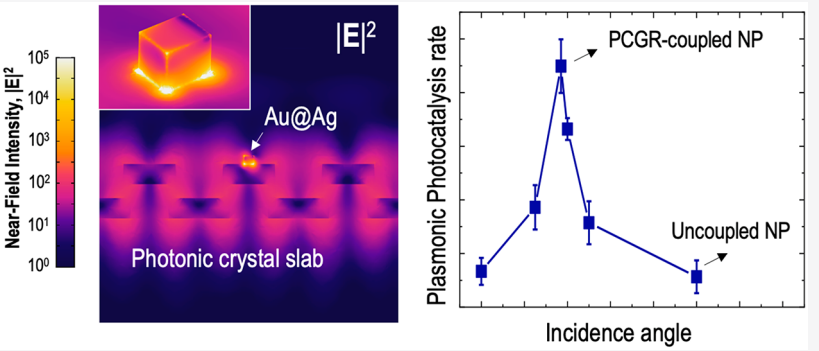

ABSTRACT: Plasmonic nanoparticles (NPs) hold tremendous promise for catalyzing light-driven chemical reactions. The conventionally assumed detrimental absorption loss from plasmon damping can now be harvested to drive chemical transformations of the NP adsorbent, through the excitation and transfer of energetic "hot" charge carriers. The rate and selectivity of plasmonic photocatalysis are dependent on the interaction between light and NPs. By engineering the strength and wavelength of the light harvesting of a NP, it is possible to achieve more efficient and selective photocatalysts. We report a plasmonic–photonic resonance hybridization strategy to substantially enhance hot electron generation at tunable, narrow-band wavelengths. By coupling the plasmon resonance of silver NPs to the guided mode resonance in a dielectric photonic crystal slab, the hot-electron-driven reduction conversion is greatly accelerated at a low illumination intensity. Broadly compatible with NPs with manifold materials and shapes that are optimized for the targeted chemistry, the generic hybrid enhancement mechanism sheds light on rational design of high-performance plasmonic photocatalysts.

KEYWORDS: *plasmonics, photocatalysis, photonic crystal, coupled mode, nanophotonics*

A new paradigm of plasmonic photocatalysis has emerged as a platform for triggering energetically intensive chemical reactions under mild temperature conditions and with potentially selective reaction pathways control.[1] Plasmonic nanoparticles (NPs) have been shown to drive molecular desorption, bond cleavage, and single- and multi-electron redox reactions on their surface.[2] Through the excitation of localized surface plasmon resonance (LSPR), a metal NP doubly functions as a nanoantenna that confines optical energy into subdiffraction volumes[3] and as a reactive element that interacts with the adsorbed molecules.[4] As a mixed light–matter mode, a plasmon polariton (PP) partially stores its energy in the kinetic motion of the free carriers, which leads to inevitable dissipative loss.[5] Besides radiative decay that re-emits a photon, a PP can nonradiatively decay through chemical interface damping where a carrier is directly excited from the metal to the molecule.[6] Alternatively, they can nonradiatively decay by exciting electron–hole pairs in the metal with certain energy distributions.[5] Ultimately, for productive chemistry to occur, the excited energetic charge carriers must be transferred to the adsorbed molecules before ultrafast carrier relaxation processes.[4] In this way, the energy in the LSPR is deposited into an adsorbed molecule, which can lead to its chemical transformations.[7]

One central quest in this emerging field is to enhance the reactivity of a plasmonic photocatalyst. The plasmonic catalytic activity is a convolution of many effects, including plasmon-derived phenomena such as near-field enhancement, absorption, and heating. In addition, the NPs' catalytic activity in the dark and lattice-derived mechanical vibrations (phonons) must

Received: June 13, 2020
Published: July 30, 2020

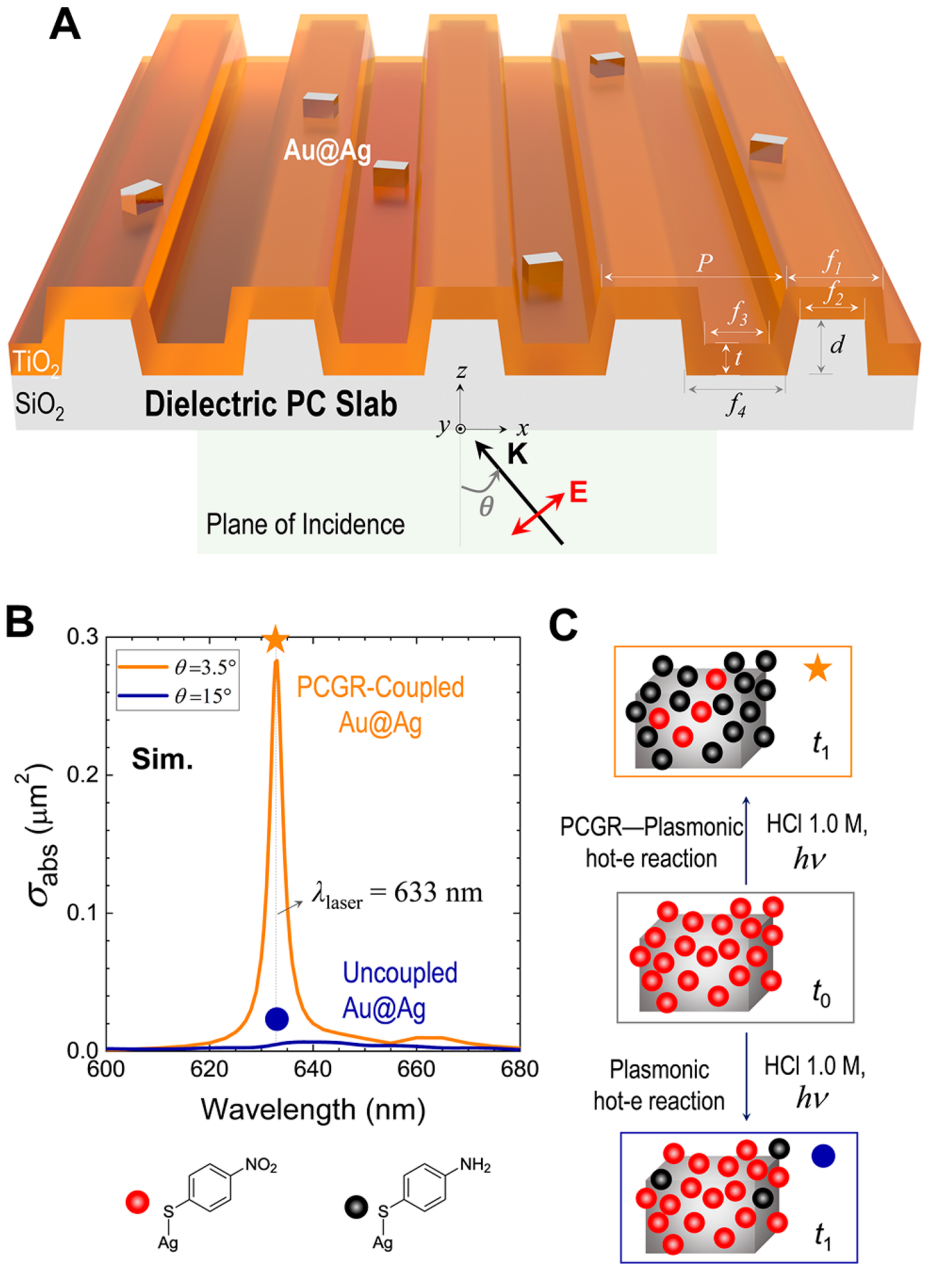

Figure 1. Design of a nanophotonic chip for enhanced plasmonic photocatalysis. (a) Plasmonic photocatalyst Au@Ag NPs are integrated onto an on-resonant dielectric photonic crystal (PC) slab to form a plasmonic−photonic hybrid. A 5 nm thick SiO_2 isolation film covering the PC surface is omitted in the schematic. The excitation laser (λ_{laser} = 633 nm) is TM-polarized (in-plane **E** field) with an incidence angle θ. Structure parameters of the PC slab: P = 380 nm, d = 130 nm, t = 76.7 nm, f_1 = 0.521, f_2 = 0.356, f_3 = 0.45, f_4 = 0.61. (b) Simulated absorption cross section σ_{abs} of an individual Au@Ag on the PC surface, when it is coupled (θ = 3.5°, orange) or uncoupled (θ = 15°, navy) to the PC guided resonance (PCGR). (c) In the presence of 1.0 M HCl, the 4-nitrothiolphenol (4-NTP) chemisorbed on Au@Ags undergo a hot-electron-mediated reduction to form 4-aminothiophenol (ATP). The PCGR-coupled conversion rate (θ = 3.5°, orange box) is much higher than that of the uncoupled cases (θ = 15°, navy box). Bottom left corner: colored labels for 4-NTP and 4-ATP.

be accounted for.[7] Recent research endeavors have been focused on engineering the NPs, including a judicious choice of its material (for example using multiple metals to separately function as the antenna and reactor sites),[8−10] size and shape (small radius of curvature is beneficial for charge transportation),[11,12] and exploration of coupled plasmonic NPs.[13−15] In this work, we introduce a novel plasmonic—photonic coupling strategy to enhance the hot electron generation in the NPs, which supplies the energy quanta to initiate a chemical reaction, at on-demand frequency bands. Our approach provides another degree of freedom by photonic hybridization, allowing for the chemical properties of the NPs to be optimized independently.

Manipulating the NPs' absorption characteristics has deep impacts on the reaction kinetics. The supralinear illumination intensity dependence of photocatalytic reaction rate in multiple plasmon-driven reactions indicates higher quantum yield with increasing photon flux.[8,16] As the field is still evolving to resolve the fundamental mechanics on hot-carrier induced activation barrier reduction, a number of experiments provide evidence that the catalyst rate is dependent on the excitation wavelength and intensity.[10,17] With an increased photon flux at

https://dx.doi.org/10.1021/acsphotonics.0c00945
ACS Photonics XXXX, XXX, XXX−XXX

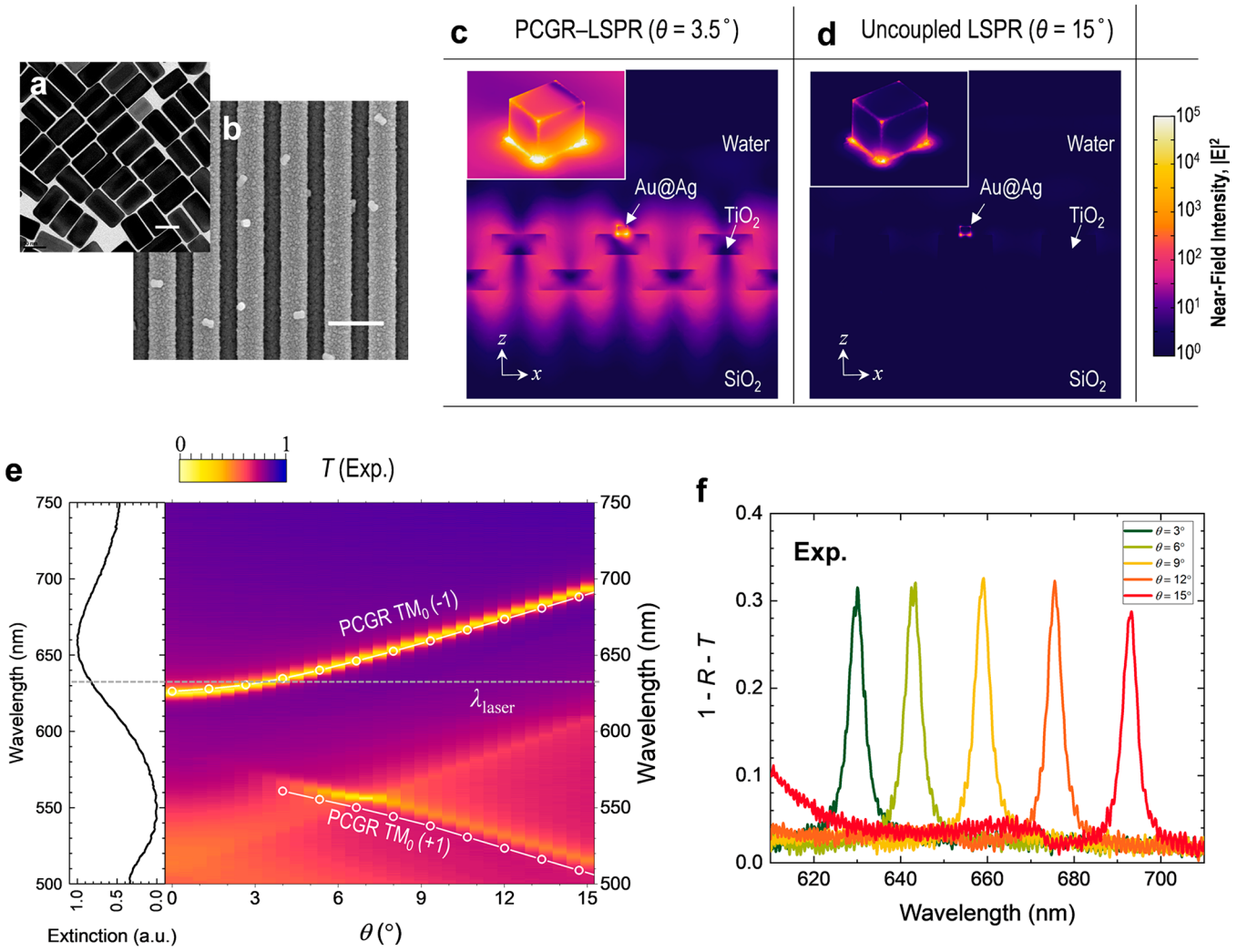

Figure 2. Optical properties of the LSPR–PCGR hybrid mode. (a) TEM image of the Au@Ag. Scale bar 50 nm. (b) Representative SEM image of the Au@Ag–PC hybrid structure. Scale bar 500 nm. (c, d) Simulated near-field intensity ($|\mathbf{E}|^2$, normalized to incidence field) of the Au@Ag–PC hybrid at (c) $\theta = 3.5°$ and (d) $\theta = 15°$. The *xz* cross-sectional slice cuts through the front surface of the Au@Ag. The insets show a close-up 3D view of the Au@Ag surface. (e) Left panel: measured extinction spectrum of Au@Ag NPs on a TiO_2-coated glass substrate immersed in water. Right panel: angle-resolved transmission spectra of the Au@Ag–PC hybrid. The simulated spectral positions of the two counterpropagating PCGRs are overlaid (white line with circular symbols). The horizontal dashed line indicates the spectral position of the excitation laser. (f) Measured (1-reflectance-transmittance) spectra of the Au@Ag–PC hybrid at various incidence angles.

the LSPR wavelength more energetic carriers are transferred into or directly excited in the metal–molecule surface species, driving it to an excited electronic state of the potential energy surface (PES) of a chemical reaction.[18] The increased reaction rate and efficiency are associated with the decreased reaction barrier in the excited state of the PES,[10] and selective reaction pathways not accessible in thermally driven catalysis are offered by new valleys in the excited PES.[19] Moreover, multicarrier photoredox reactions, which are central to artificial photosynthesis but are kinetically sluggish,[20] are only possible under very intense laser excitation, because two or more hot electrons must be simultaneously generated in a NP.[21] Therefore, the ability to amplify NP absorption power at designated wavelengths by at least 1 order of magnitude without increasing the pumping laser can be very attractive for efficient, selective plasmonic photocatalysis.

The optical response of a NP can be strongly modified by its photonic environment. A nearby optical cavity can either suppress or enhance the NP absorption through plasmonic–photonic mode hybridization.[22,23] Leveraging the cooperative coupling between the LSPR and an on-resonant photonic crystal guided resonance (PCGR),[23−25] we demonstrate greatly improved plasmon-assisted catalytic activity under very low illumination intensities. This is the first time the optical bonus from an antenna–cavity hybridization is transferred into an enhanced "chemical hotspot" through an increased hot carrier generation. Direct correlation is found between the reaction efficiency, optical absorption, and field intensity in angle-resolved measurements.

The proposed hybrid system is illustrated in Figure 1a, where gold–silver core–shell nanocuboids (Au@Ag) are supported on an optically resonant substrate, that is, a dielectric photonic crystal (PC) slab.[26] The surface is immersed in aqueous media, and the backside is excited with a transverse magnetic- (TM-) polarized laser ($\lambda_{laser} = 633$ nm) at incidence angle θ. The delocalized PCGRs in the PC slab spectrally overlap with the LSPR in the Au@Ag and the evanescent coupling between the two forms a synergistic

https://dx.doi.org/10.1021/acsphotonics.0c00945
ACS Photonics XXXX, XXX, XXX–XXX

plasmonic−photonic hybrid mode.[23,25,27,28] Numerical simulations (Figure 1b) show that the PCGR-coupled Au@Ag exhibits a sharp (line width ∼4 nm) and strongly enhanced (by ∼35× compared to NP without coupling) absorption spectrum. Moreover, the resonance wavelength can be tuned by the incidence angle. An enhanced plasmon absorption in the LSPR−PCGR coupling leads to an increased hot carrier excitation and improved plasmonic photocatalysis efficiency. We quantify this effect with a proof-of-concept hot-electron-driven reaction, where 4-nitrothiophenol (4-NTP) molecules anchored on the Au@Ag surface are onsite-reduced into 4-aminothiophenol (4-ATP) under laser excitation.[11,29] As a signature of plasmon-driven catalysis, the reaction is wavelength-dependent and exhibit highest conversion rate for the LSPR wavelength.[11,29] Here we aim to further improve the energy conversion efficiency for the optimal wavelength (633 nm). Through observation of the reaction in real-time using surface-enhanced Raman scattering (SERS), we show that the conversion ratio is dependent on the incidence angle, a direct result of plasmonic−photonic hybrid enhancement (Figure 1c).

We synthesized Au@Ag NPs as the photocatalysts, which are comprised of gold nanorods (AuNRs) as the core and silver nanocuboids as the shell,[30] as shown in the transmission electron microscopy (TEM) image in Figure 2a. The Au@Ag NPs are especially suitable for the NTP to ATP reduction because (1) the core−shell structure supports strong LSPR near λ = 633 nm, in resonance with the PCGR mode, (2) their sharp edges and tips can facilitate hot carrier transportation,[11,31] and (3) silver surface is essential to drive this reaction.[29] The Au@Ag NPs were first modified with 4-NTP molecules, where the thiols easily replace CTAC surfactant and form a self-assembled monolayer on the silver surface.[32] The NTP-modified NPs were then uniformly deposited onto a PC surface (Figure 2b). A sparse coating of 1−3 NP/μm^2 was found to be optimal, where critical coupling between the antenna and cavity leads to maximum energy absorption in NPs.[23,33] The NPs are randomly orientated, and x-orientated ones match the field polarization and will be optimally excited.[25] To avoid losing hot electrons to the underlying TiO_2, which is commonly used as an "electron filter",[34,35] a 5 nm thick SiO_2 layer was sputtered onto the PC surface before Au@Ag deposition to electronically isolate them from the TiO_2. An adjacent dielectric surface has been shown to alter the LSPR of the antenna.[36] To properly assess the LSPR of PCGR-coupled NPs, we measured the extinction of NPs coated on a SiO_2/TiO_2/glass substrate to mimic the dielectric environment of the PC surface. As shown in Figure 2e, left panel, the film-supported Au@Ag NPs exhibit a strong LSPR near 633 nm, which is red-shifted from those suspended in solution (Figure S1).

The hybrid mode is activated when satisfying the phase matching condition of the PCGR mode, whereas the LSPR mode is generally angle insensitive. This incidence angle selection rule allows direct comparison of the absorption, near-field intensity, SERS intensity, and catalytic activity between the hybrid supermode and the solitary LSPR mode. A near-field picture is helpful for understanding the coupling behavior. The hybridization at θ = 3.5° is characterized by a standing wave pattern in the PC slab and an intense optical hotspot concentrated on the Au@Ag (Figure 2c). Compared to the uncoupled case at a detuned angle (Figure 2d), the PCGR-coupled Au@Ag (Figure 2c) possesses higher electric field enhancements across the entire NP. In contrast to the plasmonic gap modes[37] where the hotspots are only accessible to a small region of the bridged NPs, our open cavity offers amplification across all the reaction sites over the Au@Ag surface. The intense electric field confined at the NP is the physical phenomenon allowing for Landau damping, which has been identified as the key mechanism to generate highly energetic carriers right at the surface, where they have access to the reactant.[38] In essence, the coupling acts as an impedance matching network that cooperatively combines the cavity's quality factor and the antenna's mode confinement.[23,33] Energy of incident photons from free space successively oscillates in a photonic microcavity, concentrates into PPs, nonradiatively decays into hot carriers, and finally transfers into molecules to alter their chemical composition.

Moreover, the spectrally tunable narrowband hybrid resonance allows matching to specific electronic transitions and production of hot carriers with specific energy distributions. Four different mechanisms have been identified for charge carrier generation through plasmon decay: interband absorption, phonon (or defect) assisted absorption, electron−electron scattering assisted absorption, and Landau damping (or surface collision assisted absorption). The excitation wavelength determines the relative contribution of each mechanism and hence the energy distribution of the generated carriers, and finally influence the energy transferred to the molecules.[39] Wavelength is therefore a key factor sculpting the reaction rate, selectivity, and pathways,[10,20] and the spectral tunability of the hybrid resonance offers additional accessibility in selective reactions. Derived from the band diagram of the PCGRs, the sharp hybrid resonance can be tuned over a broad spectral range to cover different absorption mechanisms by scanning the incidence angle (Figure 2e, right panel). In this work we target at Landau damping at the LSPR wavelength with λ_{laser} = 633 nm. The absorption enhancement is validated by measuring the angle-resolved extinction spectra 1-R-T, where R and T are the zeroth-order reflection and transmission efficiencies, respectively. Each sharp extinction peak in Figure 2f represents the hybridization at a specific incidence angle. The peak magnitude across different wavelengths follows the trend of the broadband LSPR of the uncoupled NPs as shown in Figure 2e, left panel. For a designated wavelength, the extinction can be amplified approximately 20× when hitting the resonant angle (peaks), as compared the off-resonant angles (backgrounds). The deviations from the simulation (Figure 1b) can be attributed to their discrepancy in Au@Ag density and orientations.

Once the enhanced optical hotspot was confirmed, we performed hot-electron-driven surface chemistry as described in Figure 1c. The LSPR excited in the Au@Ag undergoes nonradiative plasmon decay to generate hot carriers. A detailed reaction analysis can be found in ref 11. Briefly, six energetic electrons are generated in the NP and transferred into a 4-NTP molecule chemisorbed on the Ag surface, resulting in the terminal nitro group being reduced to an amino group.[11] The reduction requires an acid halide media (that is, HCl, HBr, and HI), where protons act as the hydrogen source and halide anions act as a hole scavenger. In the counter-half reaction, insoluble silver halide is formed and subsequent photodissociated to regenerate the silver surface.[29] A series of control experiments have demonstrated that the reaction is not induced by photothermal effects.[11,29]

https://dx.doi.org/10.1021/acsphotonics.0c00945
ACS Photonics XXXX, XXX, XXX−XXX

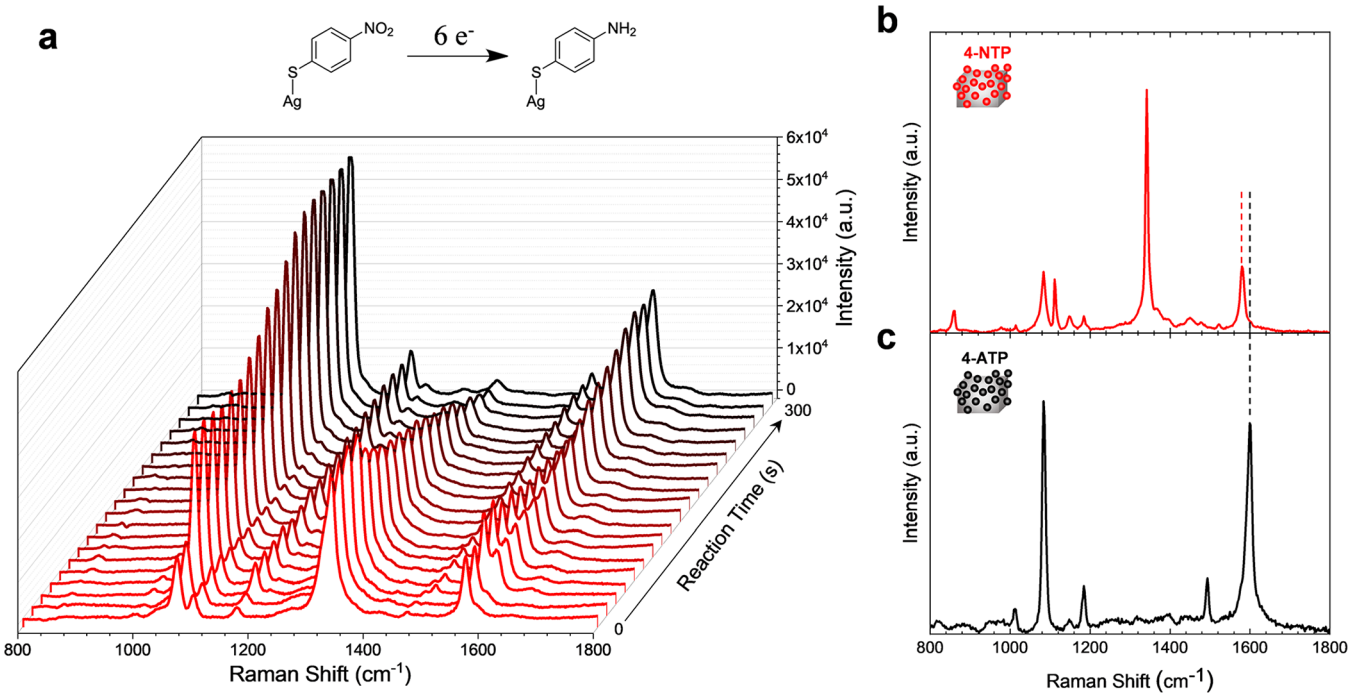

Figure 3. Real-time observation of the hot-electron-driven reaction via SERS. (a) Time-dependent SERS spectra of 4-NTP-modified Au@Ag NPs placed on a PC slab in the presence of 1.0 M HCl. Excitation parameters: incidence angle $\theta = 3.5°$, laser power 7 mW, illumination area 0.5 mm × 2 μm, integration time 2 s. The gradual line color change from red to black represents the progressive transition of 4-NTP to 4-ATP. Reference SERS spectra of (b) 4-NTP and (c) 4-ATP obtained in control experiments. The scales of vertical axes for (b) and (c) are not the same. The fingerprint Raman bands used to estimate conversion efficiency are highlighted.

Experimentally, the excitation laser stimulates chemical transformation on multiple isolated Au@Ag NPs that are sparsely distributed on the PC surface, and the molecular conversion process is observed in real time through ensembled SERS monitoring.[25] Properly orientated NPs will dominate the signal. A home-built inverted line-focusing Raman microscope[40] ensures efficient excitation of the angle-sensitive PCGR−LSPR hybrid mode. Briefly, the incident beam is focused into a line (~2 μm × 0.5 mm) oriented along the x-axis on the sample surface, and the incidence angle can be precisely adjusted (Figure S2). Note that the laser intensity used in our setup (7 $\mu W/\mu m^2$) is orders of magnitude lower than that typically used in plasmonic photocatalysis,[11,29,41] indicating the high energy efficiency emanated from mode hybridization.

We first excite the hybrid sample at the resonance angle (θ = 3.5°) and measure the evolution of SERS, as depicted in Figure 3a. The integration time for each spectrum is 2 s. We mark time zero as the time when HCl is added onto the sample surface. The time-dependent SERS spectra exhibits the dynamics of molecular bond change. The characteristic bands at 1083, 1341, and 1580 cm^{-1} at the beginning of the transformation are respectively assigned to C−S stretching, O−N−O stretching, and the phenyl-ring mode of 4-NTP.[32] With the conversion of 4-NTP to 4-ATP, the intensities of the R-NO_2-associated bands progressively decreased, and concomitantly, two characteristic bands of 4-ATP at 1493 and 1599 cm^{-1} emerged.[42] Over the course of 5 min laser excitation, most 4-NTP molecules chemisorbed on the Au@Ags were converted into 4-ATP. The SEM of Au@Ag NPs after the reaction show no obvious morphology change (Figure S8), validating the regeneration of silver in the counter-half reaction. We also measured the SERS spectra of the PCGR-coupled thiol-modified Au@Ag NPs in absence of the acid halide. The spectra for 4-NTP and 4-ATP are shown in Figure 3b and c, respectively. No reaction was observed in the absence of acid media.

We then investigate the effect of plasmonic−photonic hybridization on plasmon-assisted catalytic activity by driving the reaction at various incidence angles. The hot-electron driven reduction efficiency has a linear dependence on laser power (Figure S7). Importantly, incidence angle tuning can amplify the near-field intensity without actually increasing the laser power and would promote catalytic activities with higher efficiency. We note that the change of illumination area under the probed angles (0 to 15°) is less than 3.5%, and hence, the change in the number of irradiated NPs or the illumination intensity are negligible. A series of polydimethylsiloxane (PDMS) wells holding 1.0 M aqueous HCl media were attached to the hybrid sample surface, and each well will be probed with a distinct incidence angle θ. Since Au@Ags are uniformly distributed across the 1 × 1 cm^2 PC slab surface, it is fair to compare the reaction rates across different wells on the same chip.

After a 180 s excitation, the typical SERS spectra under six different θ are shown in Figure 4d−i, the integration time for each case is 2 s. The variance in overall SERS intensity as a function of θ is a direct result of hybrid near-field enhancement. Figure 4a shows the simulated evolution of the average electric field intensity ($|\mathbf{E}|^2 = \iint |\mathbf{E}|^2 dS / \iint dS$) at λ = 633 nm as a function of incidence angle. The resonantly coupled NP at θ = 3.5° enjoys approximately 90× higher average electric field intensity than the uncoupled case at θ = 8°, coherent with the field profiles shown in Figure 2c,d. Formally, the SERS enhancement is proportional to the product of electric field intensities at the excitation frequency

https://dx.doi.org/10.1021/acsphotonics.0c00945
ACS Photonics XXXX, XXX, XXX−XXX

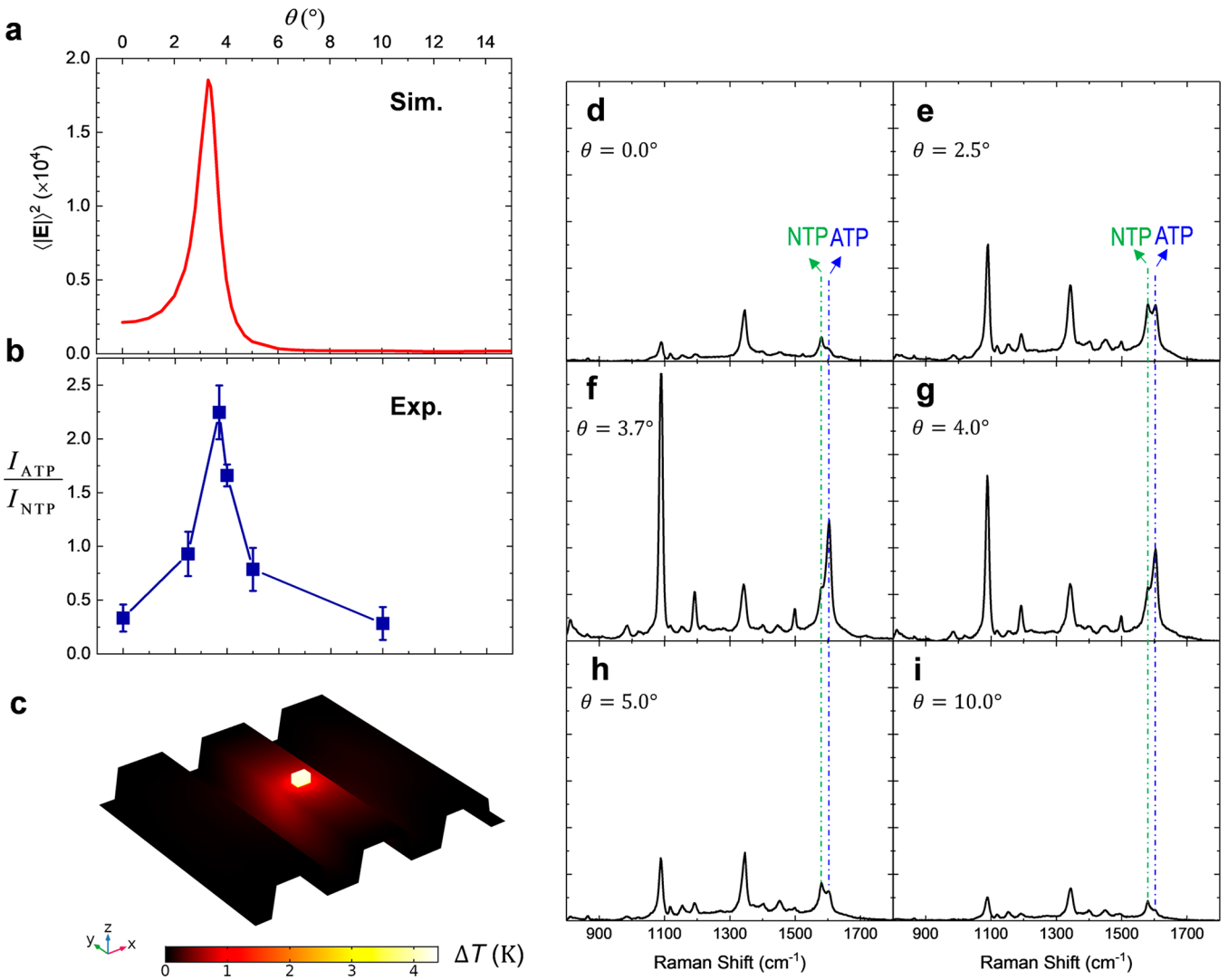

Figure 4. Enhanced hot electron photocatalysis in plasmonic−photonic coupling. (a) Simulated average near-field intensity on the surface of the Au@Ag ($\langle|\mathbf{E}|^2\rangle$, normalized to incidence field) for λ_{laser} = 633 nm as a function of incidence angle θ. (b) Experimentally obtained reaction conversion ratio (defined by the ratio of SERS intensity at 1599 and 1580 cm^{-1}) after 180 s illumination as a function of θ. (c) Simulated temperature (relative to the room temperature 293.15 K) distribution of the proposed photocatalyst surface at the LSPR−PCGR hybridization. (d−i) The SERS spectra after reaction at each θ denoted in (b). The Raman peaks utilized for calculating the conversion ratio are highlighted.

and the Raman scattering frequency.[43] In our system the SERS intensity scales only with the first term because the photonic environment for the scattered photons remains unmodified when changing excitation angles,[25] and this can be clearly seen with the angle-resolved SERS intensity of 4-NTP-modified hybrid structure in absence of acid halide (Figure S6).

The relative intensity of the SERS bands of 4-NTP and 4-ATP reflects their surface coverage rate, and we can use the ratio of 1599 and 1580 cm^{-1} band intensity to quantify the conversion efficiency. (We note that the intensity ratio between the two SERS peaks does not directly translate into molecule counts because (1) the Raman cross-section (σ) for 4-NTP and 4-ATP are not the same ($\sigma_{NTP} > \sigma_{ATP}$),[11] and (2) the result is masked by the near-field distribution (SERS enhancement factor) across the Au@Ag surface.) Figure 4d−i exhibits remarkable discrepancies in the apparent conversion efficiencies under different incidence angles. The conversion efficiency is much higher when the NPs are coupled to PCGR at θ = 3.7°, compared to LSPR operating alone at a detuned θ. We plot the conversion efficiency as a function of θ in Figure 4b. The square symbols represent average of three spots across the sample and the error bars depict the standard deviation. Remarkably, the angle-resolved behavior shows a close correlation between the numerically predicted near-field enhancements (Figure 4a) with the measured absorption amplification (Figure S5), SERS intensity (Figure S6), and photocatalysis efficiency (Figure 4b). This result demonstrates that the electromagnetic enhancements via LSPR−PCGR hybridization can be successively transferred into improved catalytic reactivity.

Hot electron excitation can be synergistic with the thermoplasmonic effects in plasmonic photocatalysis. In this study we find the hybridization-induced catalysis activity enhancement has an electronic origin, because the very low incidence intensity and good thermal conductivity do not induce adequate temperature increase. We conducted thermal simulations (COMSOL) to estimate the temperature around the PCGR-coupled Au@Ag. Briefly, the power adsorbed by the Au@Ag (obtained as the product of absorption cross section and illumination intensity) was input into a steady-state heat

https://dx.doi.org/10.1021/acsphotonics.0c00945
ACS Photonics XXXX, XXX, XXX−XXX

transfer model as a volumetric heat source.[44,45] The temperature profile of the photocatalysts surface is shown in Figure 4c. The numerical model predicts a small temperature rise (<5 °C) in the Au@Ag, which is quantitatively in line with the reported single-particle nano thermometry measurements (detailed in Supporting Information).[39] This mild thermal effect is unlikely to have any significant effects on the chemical reaction. Therefore, the improved photocatalytic activity can be ascribed to the increased hot electron generation rate through hybrid absorption enhancement. Higher production rate of energetic carriers in the Au@Ag leads to a higher flux of hot electrons transferred into the adsorbed 4-NTP molecules, and as a result accelerates the reduction process. We note that, as a general scheme to more efficiently couple light into NPs, our PCGR hybridizing approach is also applicable to boost direct energy transfer from metal to molecules based on chemical interface damping.

In summary, we have demonstrated a new approach to enhance the plasmon-assisted catalytic activity through coupling plasmonic NPs to a photonic microcavity resonator. Through forming an intense optical hotspot at the NP, the LSPR–PCGR hybridization significantly enhances the hot carrier generation at selected narrowband wavelengths, while simultaneously possessing broad spectral tunability. We have shown that the energy conversion efficiency can be boosted by over 1 order of magnitude. The PCGR-coupling strategy is widely compatible with a variety of NPs, allowing for independent control of optical–chemical properties. The fabrication of the PC surface is readily scalable with nanoimprint lithography, making the hybrid strategy attractive for practical use in industrial photocatalysis.

■ ASSOCIATED CONTENT

Supporting Information

The Supporting Information is available free of charge at https://pubs.acs.org/doi/10.1021/acsphotonics.0c00945.

Materials and methods (fabrication of PC slabs, synthesis of Au@Ags, Au@Ag surface modification, Au@Ag–PC integration, extinction measurement, electron microscopy characterizations, angle-resolved Raman microscope), numerical simulations (electromagnetic and thermal modeling in COMSOL Multiphysics), and additional data (absorption enhancement, SERS intensity as a function of incidence angle, power dependence of hot electron reaction, SEM of Au@Ag after reaction) (PDF)

■ AUTHOR INFORMATION

Corresponding Author

Brian T. Cunningham − *Department of Electrical and Computer Engineering, Holonyak Micro and Nanotechnology Laboratory, Carl R. Woese Institute for Genomic Biology, and Department of Bioengineering, University of Illinois at Urbana–Champaign, Urbana, Illinois 61801, United States*; Email: bcunning@illinois.edu

Authors

Qinglan Huang − *Department of Electrical and Computer Engineering and Holonyak Micro and Nanotechnology Laboratory, University of Illinois at Urbana–Champaign, Urbana, Illinois 61801, United States*; orcid.org/0000-0001-8337-1947

Taylor D. Canady − *Holonyak Micro and Nanotechnology Laboratory and Carl R. Woese Institute for Genomic Biology, University of Illinois at Urbana–Champaign, Urbana, Illinois 61801, United States*

Rohit Gupta − *Department of Mechanical Engineering and Materials Science, Washington University in St. Louis, St. Louis, Missouri 63130, United States*

Nantao Li − *Department of Electrical and Computer Engineering and Holonyak Micro and Nanotechnology Laboratory, University of Illinois at Urbana–Champaign, Urbana, Illinois 61801, United States*

Srikanth Singamaneni − *Department of Mechanical Engineering and Materials Science, Washington University in St. Louis, St. Louis, Missouri 63130, United States*; orcid.org/0000-0002-7203-2613

Complete contact information is available at: https://pubs.acs.org/10.1021/acsphotonics.0c00945

Notes

The authors declare no competing financial interest.

■ ACKNOWLEDGMENTS

This work was supported by the National Science Foundation, Grant NSF CBET 19-00277. Q.H. acknowledges the Sah Doctoral Fellowship from UIUC ECE. T.D.C. is supported by an Institute for Genomic Biology (IGB) fellowship.

■ REFERENCES

(1) Aslam, U.; Rao, V. G.; Chavez, S.; Linic, S. Catalytic conversion of solar to chemical energy on plasmonic metal nanostructures. *Nat. Catal* **2018**, *1* (9), 656–665.

(2) Zhang, Y.; He, S.; Guo, W.; Hu, Y.; Huang, J.; Mulcahy, J. R.; Wei, W. D. Surface-Plasmon-Driven Hot Electron Photochemistry. *Chem. Rev.* **2018**, *118* (6), 2927–2954.

(3) Maier, S. A. Localized Surface Plasmons. *Plasmonics: Fundamentals and Applications*; Springer US: New York, NY, 2007; pp 65–88.

(4) Brongersma, M. L.; Halas, N. J.; Nordlander, P. Plasmon-induced hot carrier science and technology. *Nat. Nanotechnol.* **2015**, *10*, 25.

(5) Khurgin, J. B. How to deal with the loss in plasmonics and metamaterials. *Nat. Nanotechnol.* **2015**, *10*, 2.

(6) Kazuma, E.; Jung, J.; Ueba, H.; Trenary, M.; Kim, Y. Real-space and real-time observation of a plasmon-induced chemical reaction of a single molecule. *Science* **2018**, *360* (6388), 521.

(7) Gargiulo, J.; Berté, R.; Li, Y.; Maier, S. A.; Cortés, E. From Optical to Chemical Hot Spots in Plasmonics. *Acc. Chem. Res.* **2019**, *52* (9), 2525–2535.

(8) Swearer, D. F.; Zhao, H.; Zhou, L.; Zhang, C.; Robatjazi, H.; Martirez, J. M. P.; Krauter, C. M.; Yazdi, S.; McClain, M. J.; Ringe, E.; Carter, E. A.; Nordlander, P.; Halas, N. J. Heterometallic antenna–reactor complexes for photocatalysis. *Proc. Natl. Acad. Sci. U. S. A.* **2016**, *113* (32), 8916.

(9) Aslam, U.; Chavez, S.; Linic, S. Controlling energy flow in multimetallic nanostructures for plasmonic catalysis. *Nat. Nanotechnol.* **2017**, *12*, 1000.

(10) Zhou, L.; Swearer, D. F.; Zhang, C.; Robatjazi, H.; Zhao, H.; Henderson, L.; Dong, L.; Christopher, P.; Carter, E. A.; Nordlander, P.; Halas, N. J. Quantifying hot carrier and thermal contributions in plasmonic photocatalysis. *Science* **2018**, *362* (6410), 69.

(11) Cortés, E.; Xie, W.; Cambiasso, J.; Jermyn, A. S.; Sundararaman, R.; Narang, P.; Schlücker, S.; Maier, S. A. Plasmonic hot electron transport drives nano-localized chemistry. *Nat. Commun.* **2017**, *8* (1), 14880.

(12) Reineck, P.; Brick, D.; Mulvaney, P.; Bach, U. Plasmonic Hot Electron Solar Cells: The Effect of Nanoparticle Size on Quantum Efficiency. *J. Phys. Chem. Lett.* **2016**, *7* (20), 4137−4141.
(13) Simoncelli, S.; Li, Y.; Cortés, E.; Maier, S. A. Imaging Plasmon Hybridization of Fano Resonances via Hot-Electron-Mediated Absorption Mapping. *Nano Lett.* **2018**, *18* (6), 3400−3406.
(14) de Nijs, B.; Benz, F.; Barrow, S. J.; Sigle, D. O.; Chikkaraddy, R.; Palma, A.; Carnegie, C.; Kamp, M.; Sundararaman, R.; Narang, P.; Scherman, O. A.; Baumberg, J. J. Plasmonic tunnel junctions for single-molecule redox chemistry. *Nat. Commun.* **2017**, *8* (1), 994.
(15) Shi, X.; Ueno, K.; Oshikiri, T.; Sun, Q.; Sasaki, K.; Misawa, H. Enhanced water splitting under modal strong coupling conditions. *Nat. Nanotechnol.* **2018**, *13* (10), 953−958.
(16) Christopher, P.; Xin, H.; Marimuthu, A.; Linic, S. Singular characteristics and unique chemical bond activation mechanisms of photocatalytic reactions on plasmonic nanostructures. *Nat. Mater.* **2012**, *11*, 1044.
(17) Kim, Y.; Dumett Torres, D.; Jain, P. K. Activation Energies of Plasmonic Catalysts. *Nano Lett.* **2016**, *16* (5), 3399−3407.
(18) Cortés, E. Activating plasmonic chemistry. *Science* **2018**, *362* (6410), 28.
(19) Zhang, X.; Li, X.; Zhang, D.; Su, N. Q.; Yang, W.; Everitt, H. O.; Liu, J. Product selectivity in plasmonic photocatalysis for carbon dioxide hydrogenation. *Nat. Commun.* **2017**, *8* (1), 14542.
(20) Yu, S.; Wilson, A. J.; Heo, J.; Jain, P. K. Plasmonic Control of Multi-Electron Transfer and C−C Coupling in Visible-Light-Driven CO2 Reduction on Au Nanoparticles. *Nano Lett.* **2018**, *18* (4), 2189−2194.
(21) Kim, Y.; Smith, J. G.; Jain, P. K. Harvesting multiple electron−hole pairs generated through plasmonic excitation of Au nanoparticles. *Nat. Chem.* **2018**, *10* (7), 763−769.
(22) Heylman, K. D.; Thakkar, N.; Horak, E. H.; Quillin, S. C.; Cherqui, C.; Knapper, K. A.; Masiello, D. J.; Goldsmith, R. H. Optical microresonators as single-particle absorption spectrometers. *Nat. Photonics* **2016**, *10* (12), 788−795.
(23) Huang, Q.; Cunningham, B. T. Microcavity-Mediated Spectrally Tunable Amplification of Absorption in Plasmonic Nanoantennas. *Nano Lett.* **2019**, *19* (8), 5297−5303.
(24) Fan, S. H.; Joannopoulos, J. D. Analysis of guided resonances in photonic crystal slabs. *Phys. Rev. B: Condens. Matter Mater. Phys.* **2002**, *65* (23), 235112.
(25) Liu, J. N.; Huang, Q.; Liu, K. K.; Singamaneni, S.; Cunningham, B. T. Nanoantenna-Microcavity Hybrids with Highly Cooperative Plasmonic-Photonic Coupling. *Nano Lett.* **2017**, *17* (12), 7569−7577.
(26) Joannopoulos, J. D.; Johnson, S. G.; Winn, J. N.; Meade, R. D. *Photonic Crystals: Molding the Flow of Light*; Princeton University Press, 2011.
(27) Canady, T. D.; Li, N.; Smith, L. D.; Lu, Y.; Kohli, M.; Smith, A. M.; Cunningham, B. T. Digital-resolution detection of microRNA with single-base selectivity by photonic resonator absorption microscopy. *Proc. Natl. Acad. Sci. U. S. A.* **2019**, *116* (39), 19362.
(28) Che, C.; Li, N.; Long, K. D.; Aguirre, M. Á.; Canady, T. D.; Huang, Q.; Demirci, U.; Cunningham, B. T. Activate capture and digital counting (AC + DC) assay for protein biomarker detection integrated with a self-powered microfluidic cartridge. *Lab Chip* **2019**, *19*, 3943.
(29) Xie, W.; Schlücker, S. Hot electron-induced reduction of small molecules on photorecycling metal surfaces. *Nat. Commun.* **2015**, *6* (1), 7570.
(30) Liu, K.-K.; Tadepalli, S.; Tian, L.; Singamaneni, S. Size-Dependent Surface Enhanced Raman Scattering Activity of Plasmonic Nanorattles. *Chem. Mater.* **2015**, *27* (15), 5261−5270.
(31) Giugni, A.; Torre, B.; Toma, A.; Francardi, M.; Malerba, M.; Alabastri, A.; Proietti Zaccaria, R.; Stockman, M. I.; Di Fabrizio, E. Hot-electron nanoscopy using adiabatic compression of surface plasmons. *Nat. Nanotechnol.* **2013**, *8*, 845.
(32) Huang, J.; Zhu, Y.; Lin, M.; Wang, Q.; Zhao, L.; Yang, Y.; Yao, K. X.; Han, Y. Site-Specific Growth of Au−Pd Alloy Horns on Au Nanorods: A Platform for Highly Sensitive Monitoring of Catalytic Reactions by Surface Enhancement Raman Spectroscopy. *J. Am. Chem. Soc.* **2013**, *135* (23), 8552−8561.
(33) Haus, H. A. *Waves and Fields in Optoelectronics*; Prentice-Hall, 1984.
(34) Mubeen, S.; Lee, J.; Singh, N.; Krämer, S.; Stucky, G. D.; Moskovits, M. An autonomous photosynthetic device in which all charge carriers derive from surface plasmons. *Nat. Nanotechnol.* **2013**, *8*, 247.
(35) Zheng, B. Y.; Zhao, H.; Manjavacas, A.; McClain, M.; Nordlander, P.; Halas, N. J. Distinguishing between plasmon-induced and photoexcited carriers in a device geometry. *Nat. Commun.* **2015**, *6* (1), 7797.
(36) Knight, M. W.; Wu, Y.; Lassiter, J. B.; Nordlander, P.; Halas, N. J. Substrates Matter: Influence of an Adjacent Dielectric on an Individual Plasmonic Nanoparticle. *Nano Lett.* **2009**, *9* (5), 2188−2192.
(37) Baumberg, J. J.; Aizpurua, J.; Mikkelsen, M. H.; Smith, D. R. Extreme nanophotonics from ultrathin metallic gaps. *Nat. Mater.* **2019**, *18* (7), 668−678.
(38) Khurgin, J. B. Hot carriers generated by plasmons: where are they generated and where do they go from there? *Faraday Discuss.* **2019**, *214* (0), 35−58.
(39) Pensa, E.; Gargiulo, J.; Lauri, A.; Schlücker, S.; Cortés, E.; Maier, S. A. Spectral Screening of the Energy of Hot Holes over a Particle Plasmon Resonance. *Nano Lett.* **2019**, *19* (3), 1867−1874.
(40) Palonpon, A. F.; Ando, J.; Yamakoshi, H.; Dodo, K.; Sodeoka, M.; Kawata, S.; Fujita, K. Raman and SERS microscopy for molecular imaging of live cells. *Nat. Protoc.* **2013**, *8*, 677.
(41) Benz, F.; Schmidt, M. K.; Dreismann, A.; Chikkaraddy, R.; Zhang, Y.; Demetriadou, A.; Carnegie, C.; Ohadi, H.; de Nijs, B.; Esteban, R.; Aizpurua, J.; Baumberg, J. J. Single-molecule optomechanics in "picocavities. *Science* **2016**, *354* (6313), 726.
(42) Huang, Y.-F.; Zhu, H.-P.; Liu, G.-K.; Wu, D.-Y.; Ren, B.; Tian, Z.-Q. When the Signal Is Not from the Original Molecule To Be Detected: Chemical Transformation of para-Aminothiophenol on Ag during the SERS Measurement. *J. Am. Chem. Soc.* **2010**, *132* (27), 9244−9246.
(43) Ding, S.-Y.; Yi, J.; Li, J.-F.; Ren, B.; Wu, D.-Y.; Panneerselvam, R.; Tian, Z.-Q. Nanostructure-based plasmon-enhanced Raman spectroscopy for surface analysis of materials. *Nature Reviews Materials* **2016**, *1*, 16021.
(44) Mauser, K. W.; Kim, S.; Mitrovic, S.; Fleischman, D.; Pala, R.; Schwab, K. C.; Atwater, H. A. Resonant thermoelectric nanophotonics. *Nat. Nanotechnol.* **2017**, *12*, 770.
(45) Baffou, G.; Quidant, R.; García de Abajo, F. J. Nanoscale Control of Optical Heating in Complex Plasmonic Systems. *ACS Nano* **2010**, *4* (2), 709−716.

https://dx.doi.org/10.1021/acsphotonics.0c00945
ACS Photonics XXXX, XXX, XXX−XXX